Cell Reports, Volume *43*

Supplemental information

Baf155 controls hematopoietic differentiation and regeneration through chromatin priming

Jun Wu, Changxu Fan, Ashraf Ul Kabir, Karen Krchma, Minseo Kim, Yoojung Kwon, Xiaoyun Xing, Ting Wang, and Kyunghee Choi

A

Mating Scheme	# of Litters	# of pups	avg litter size (g)	Expected KOs(25%)	# of KOs	Viability of KOs
♂ Baf155 f/f x ♀ Vav(+); Baf155 f/+	103	553	5.3	138.25	84	~15%

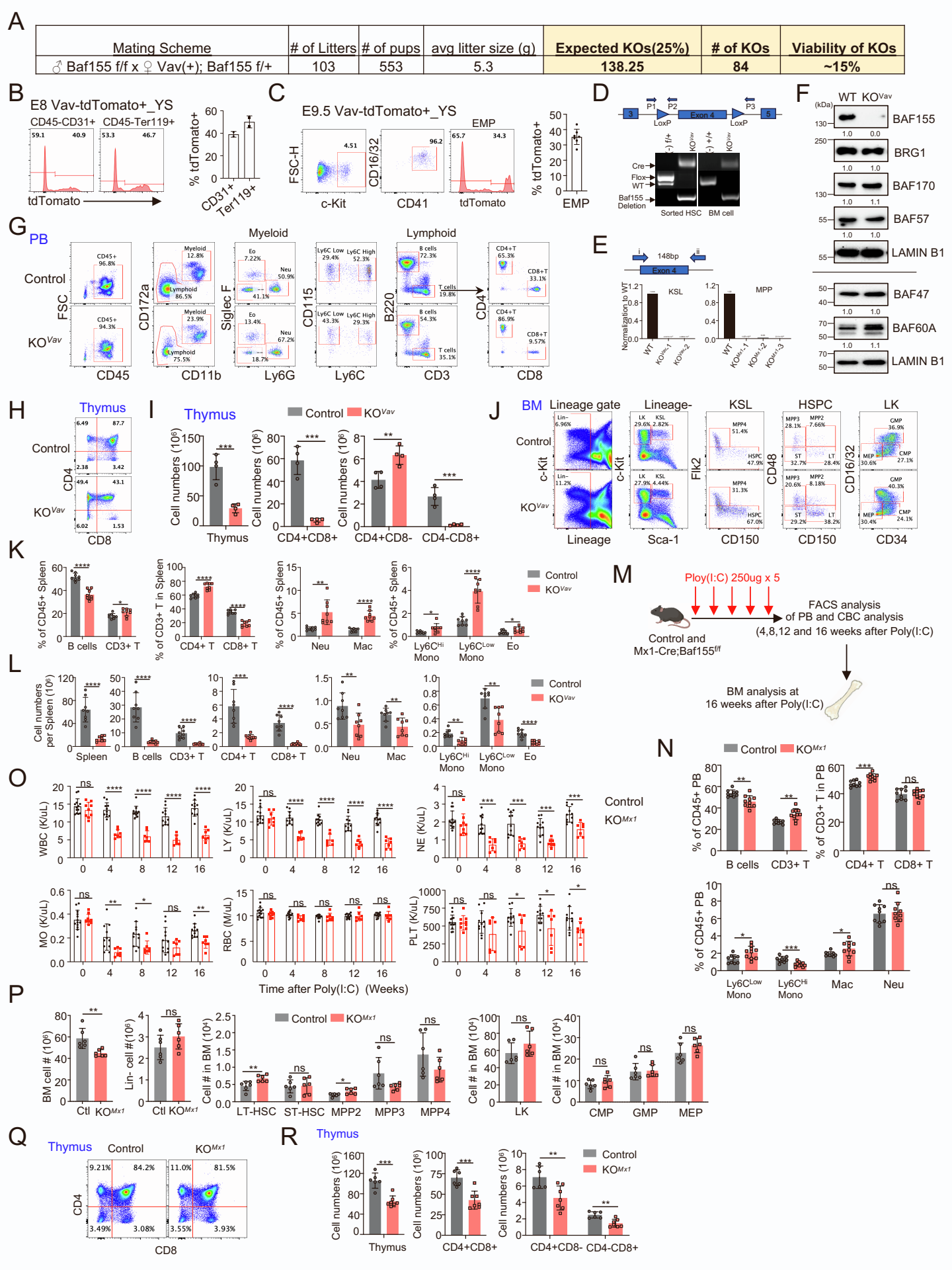

Figure S1. *Baf155* KO mice show cytopenia at steady-state hematopoiesis, related to Figure 1.

(A) The results are presented as the actual versus expected viability and numbers of the *Baf155 KO^{Vav}* mice.

(B) Flow cytometry analysis of endothelial (CD45-CD31+) and erythroid cells (CD45-TER119+) from E8 *Vav-Cre; Rosa26-floxed stop-tdTomato* YS. The representative FACS plots are shown in the left panel. The percentage of tdTomato+ cells is shown in the right panel (n=2).

(C) Flow cytometry analysis of EMP (cKit+CD41+CD16/32+) from E9.5 *Vav-Cre; Rosa26-floxed stop-tdTomato* YS. The representative FACS plots are shown in the left panel. The percentage of tdTomato+ cells is shown in the right panel (n=7).

(D) Genotyping of sorted HSC and BM cells from Control and *Baf155 KO^{Vav}* mice to evaluate *Baf155* deletion efficiency. The overview of the conditional *Baf155*-flox allele was shown on the top panel. HSCs are sorted as: CD34^{-}CD48^{-} CD150^{+}KSL.

(**E**) Genomic quantitative PCR shows the *Baf155* deletion efficiency in KSL cells from *Baf155 KO^{Vav}* mice and MPP cells from *Baf155 KO^{Mx1}* mice. The genomic deletion of *Baf155* was normalized to that of the WT. MPPs are sorted as: CD48+CD150-KSL.

(F) Western blot analysis shows the protein expression of BAF155, BRG1, BAF170, BAF57, BAF47 and BAF60A in BM cells from control and *Baf155 KO^{Vav}* mice (The value was shown as normalization to LAMIN B1 and compared to WT).

(G) The representative flow cytometry analysis of different lineage compartments in PB of control and *Baf155 KO^{Vav}* mice at steady-state hematopoiesis.

(H) Flow cytometry analysis of co-receptor expression in thymus of control and *Baf155 KO^{Vav}* mice (About 1 month old).

(I) The cell numbers of different T cell populations in the thymus of control (n=4) and *Baf155 KO^{Vav}* (n=4) mice as determined by flow cytometry are shown.

(J) The representative flow cytometry analysis of different progenitors in the BM of control and *Baf155 KO^{Vav}* mice at steady-state hematopoiesis.

(K, L) Different lineages percentage **(K)** and numbers **(L)** in the spleen of control and *Baf155 KO^{Vav}* mice were analyzed by flow cytometry. Control (n=8) and *Baf155 KO^{Vav}* (n=8).

(M) Schematic of workflow to induce deletion of *Baf155* in adult *Baf155 KO^{Mx1}* mice with poly (I:C).

(N) Different lineages percentages in the PB of control (n=9) and Baf155 KOMx1 (n=10) mice were analyzed by flow cytometry at 1st month after poly (I:C) induction.

(O) Complete blood count (CBC) analysis of peripheral blood (PB) from control (n=11) and *Baf155 KO^{Mx1}* (n=7) mice at different time point after poly (I:C) induction.

(P) Total BM cellularity and different hematopoietic progenitors in BM of control (n=6) and *Baf155 KO^{Mx1}* (n=6) mice were measured by flow cytometry at 16 weeks after poly (I:C) induction.

(Q) Flow cytometry analysis of co-receptor expression in thymus of control and *Baf155 KO^{Mx1}* mice at 1st month after poly (I:C) induction.

(R) The cell numbers of different T cell populations in the thymus of control (n=6) and *Baf155 KO^{Mx1}* (n=7) mice as determined by flow cytometry are shown.

In all relevant panels, each symbol represents an individual embryo or mouse. For all graphs, data are presented as mean±SD, and p value were determined by unpaired two-tailed Student's t test. n.s. not significant, *$p<0.05$, **$p<0.005$, ***$p<0.001$, ****$p<0.0001$.

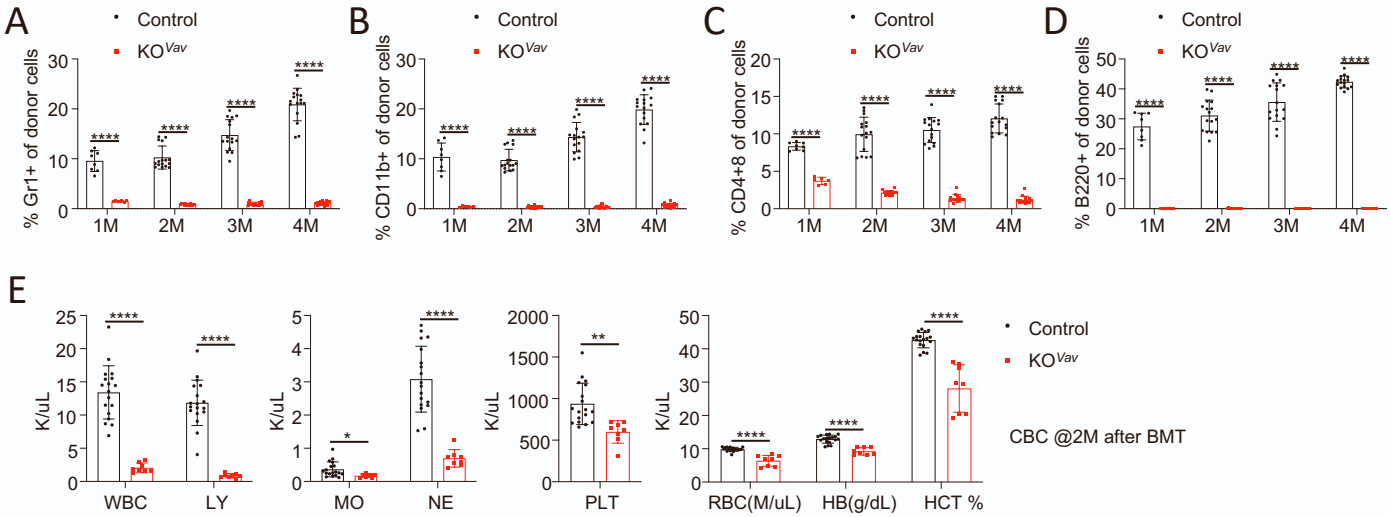

Figure S2. *Baf155*-deficient BMs display defective reconstitution ability, related to Figure 2.

(A-D) Percentage of donor-derived granulocytes (Gr1) **(A)**, monocytes (CD11b) **(B)**, T cells (CD4+8) **(C)** and B cells (B220) **(D)** in the PB of recipient mice at different time point after total BM cells competitive transplantation. Control (n=16) and *Baf155 KO^{Vav}* (n=15).

(E) Complete blood count (CBC) analysis of peripheral blood (PB) from recipient mice 60 days after non-competitive total BM transplantation. Control (n=18) and *Baf155 KO^{Vav}* (n=8) mice.

In all relevant panels, each symbol represents an individual mouse. For all graphs, data are presented as mean±SD, and p value were determined by unpaired two-tailed Student's t test. **p<0.05, **p<0.005, ***p<0.001, ****p<0.0001.*

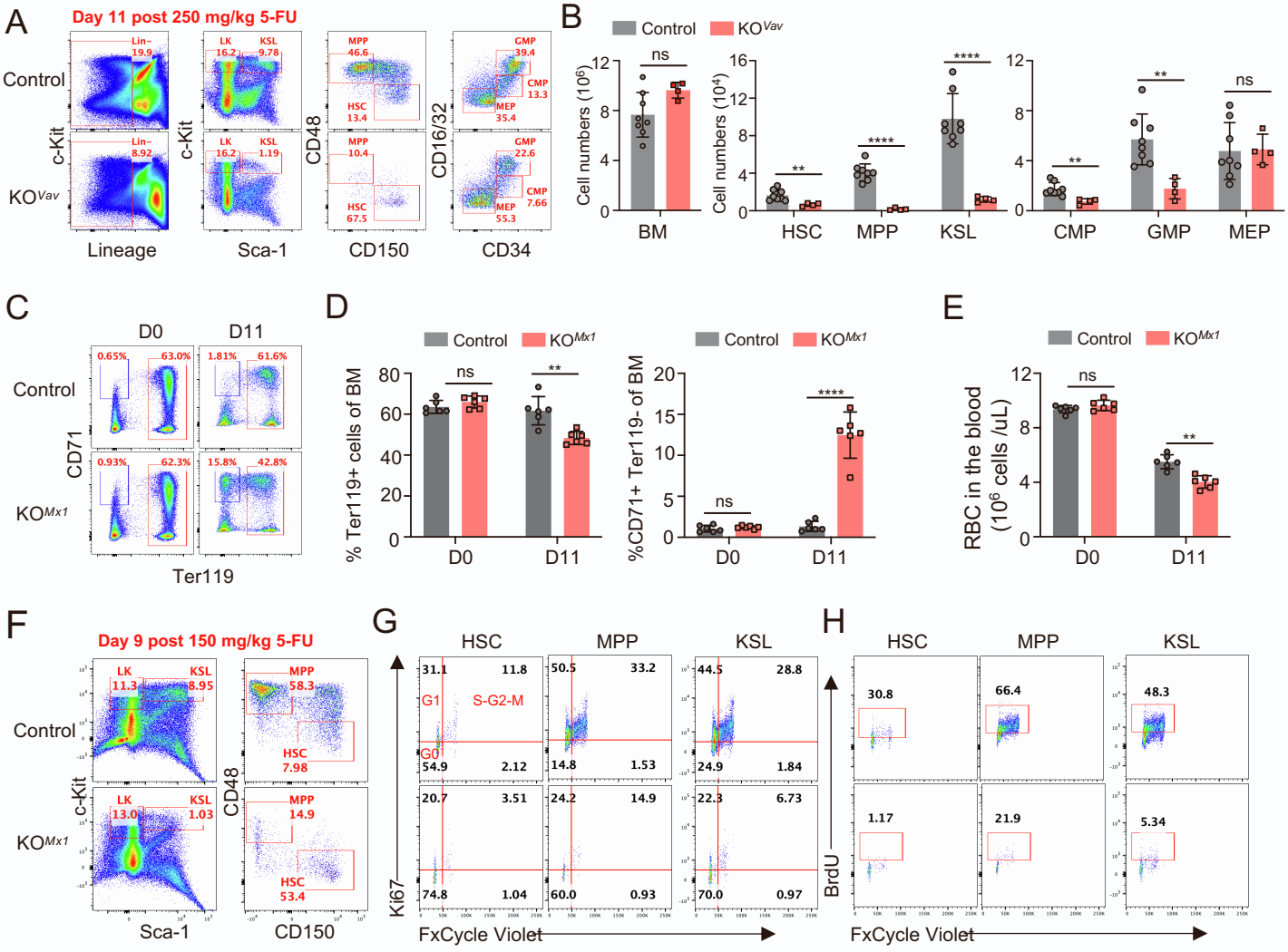

Figure S3. *Baf155*-deficient impairs HSC regeneration upon 5-FU injury, related to Figure 3.

(A, B) Analysis of different hematopoietic progenitors in BM of control (n=8) and *Baf155 KO^{Vav}* (n=4) mice treated with one dose of 250mg/kg 5-FU at D11. The representative flow cytometry analysis is shown in **(A)**, and BM cellularity and cell numbers of different hematopoietic progenitors are shown at **(B)**.

(C, D) Representative flow cytometry analyses **(C)** and quantification **(D)** of Ter119+, CD71+Ter119- population from BM of 5-FU treated control (n=6) and *Baf155 KO^{Mx1}* (n=6) mice at day 11.

(E) Red blood cell (RBC) counts from peripheral blood (PB) of 5-FU treated control (n=6) and *Baf155 KO^{Mx1}* (n=6) mice at day 11.

(F) The representative flow cytometry analysis of KSLs, MPPs and HSCs from 150mg/kg 5-FU treated control and *Baf155 KO^{Mx1}* mice at day 9 are shown.

(G) The representative cell cycle analysis of HSCs, MPPs and KSLs from 150mg/kg 5-FU treated control and *Baf155 KO^{Mx1}* mice at day 9 as determined by Ki67 and FxCycle staining are shown.

(H) The representative BrdU+ in HSCs, MPPs and KSLs cells from 150mg/kg 5-FU treated control and *Baf155 KO^{Mx1}* mice at day 9 as determined by in vivo BrdU assay are shown.

In all relevant panels, each symbol represents an individual mouse. For all graphs, data are presented as mean±SD, and p value were determined by unpaired two-tailed Student's t test. ***p<0.005, ****p<0.0001.*

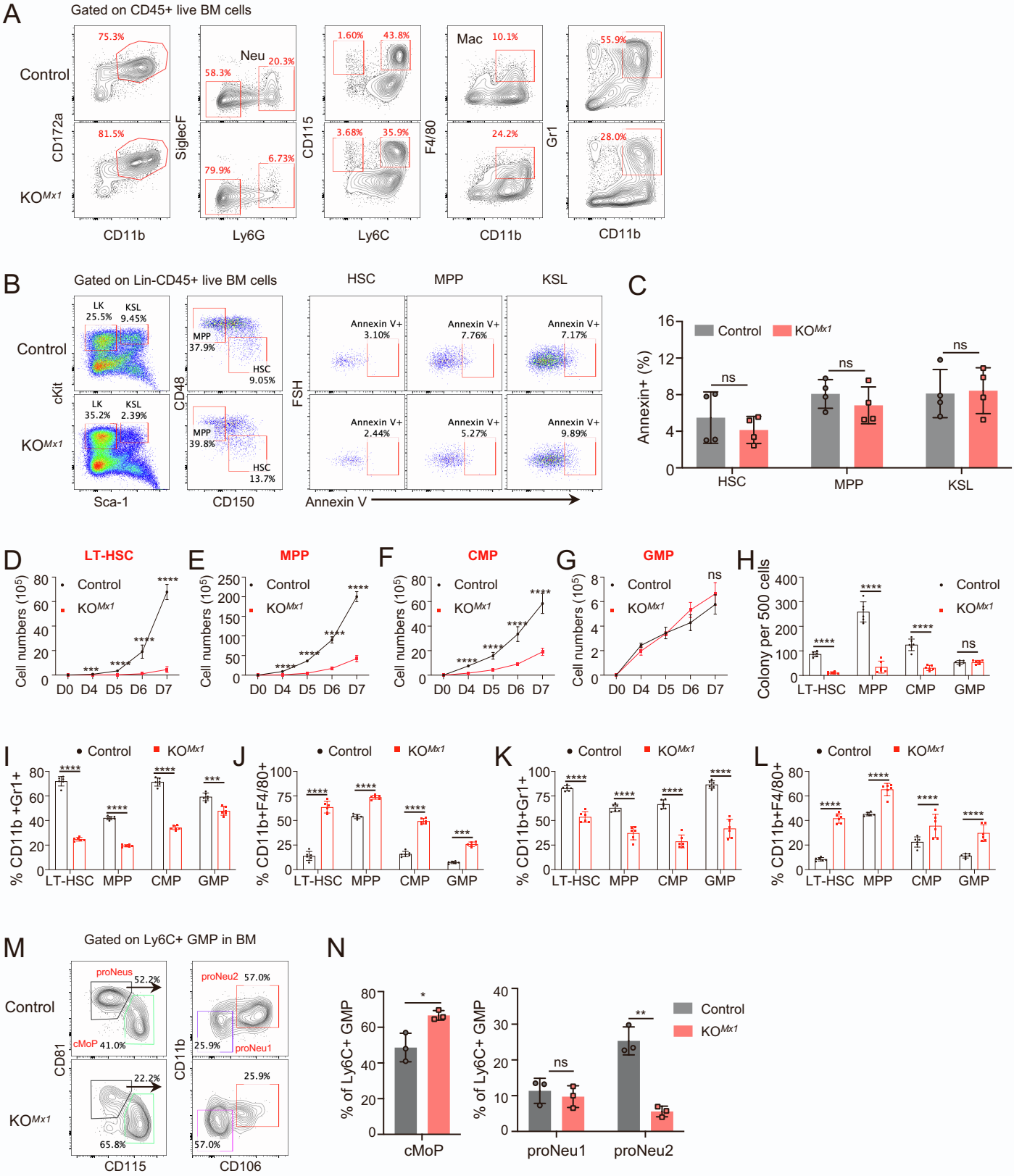

Figure S4. *Baf155*-deficient HSPCs show macrophage-skewed myeloid differentiation, related to Figure 4.

(A) The representative flow cytometry analysis of different lineage compartments in the BM of Control and *Baf155 KO^{Mx1}* mice after Cy+2G-CSF treatment.

(B, C) The representative apoptotic analysis (**B**) and quantification (**C**) of different progenitors in the BM of Control and *Baf155 KO^{Mx1}* mice after Cy+2G-CSF treatment.

(D-G) Cell numbers of ex-vivo-cultured LT-HSCs (CD34^{-}Flk2^{-} KSL cells) **(D)**, MPPs (Flk2^{hi} CD34^{+} KSL cells) **(E)**, CMPs (CD34^{+}CD16/32^{-} LK cells) **(F)**, GMPs (CD34^{+}CD16/32^{+} LK cells) **(G)** at different time points in liquid media with combination of cytokines SCF+FLT3L+mTPO+IL3+ IL6+IL11+M-CSF+GM-CSF. Control (n=6) and *Baf155 KO^{Mx1}* (n=6).

(H) Colony numbers per 500 cells input were counted 6 days after plating in M3434 methylcellulose. control (n=6) and *Baf155 KO^{Mx1}* (n=6).

(I, J) Flow cytometry analysis of the frequency of CD11b^{+}Gr1^{+} cells **(I)** and CD11b^{+}F4/80^{+} cells **(J)** after 7-day culture in liquid media. Control (n=6) and *Baf155 KO^{Mx1}* (n=6).

(K, L) Flow cytometry analysis of the frequency of CD11b^{+}Gr1^{+} cells **(K)** and CD11b^{+}F4/80^{+} cells **(L)** after cells were replated in M3434 methylcellulose at day 6. Control (n=6) and *Baf155 KO^{Mx1}* (n=6).

(M, N) The representative flow cytometry analysis (**M**) and quantification (**N**) of cMoP, proNeu1 and proNeu2 in control (n=3) and *Baf155 KO^{Mx1}*(n=3) mice. cMoP=common monocyte progenitor.

In all relevant panels, each symbol represents an individual mouse. For all graphs, data are presented as mean±SD, and p value were determined by unpaired two-tailed Student's t test. n.s. not significant, *****p<0.0001.*

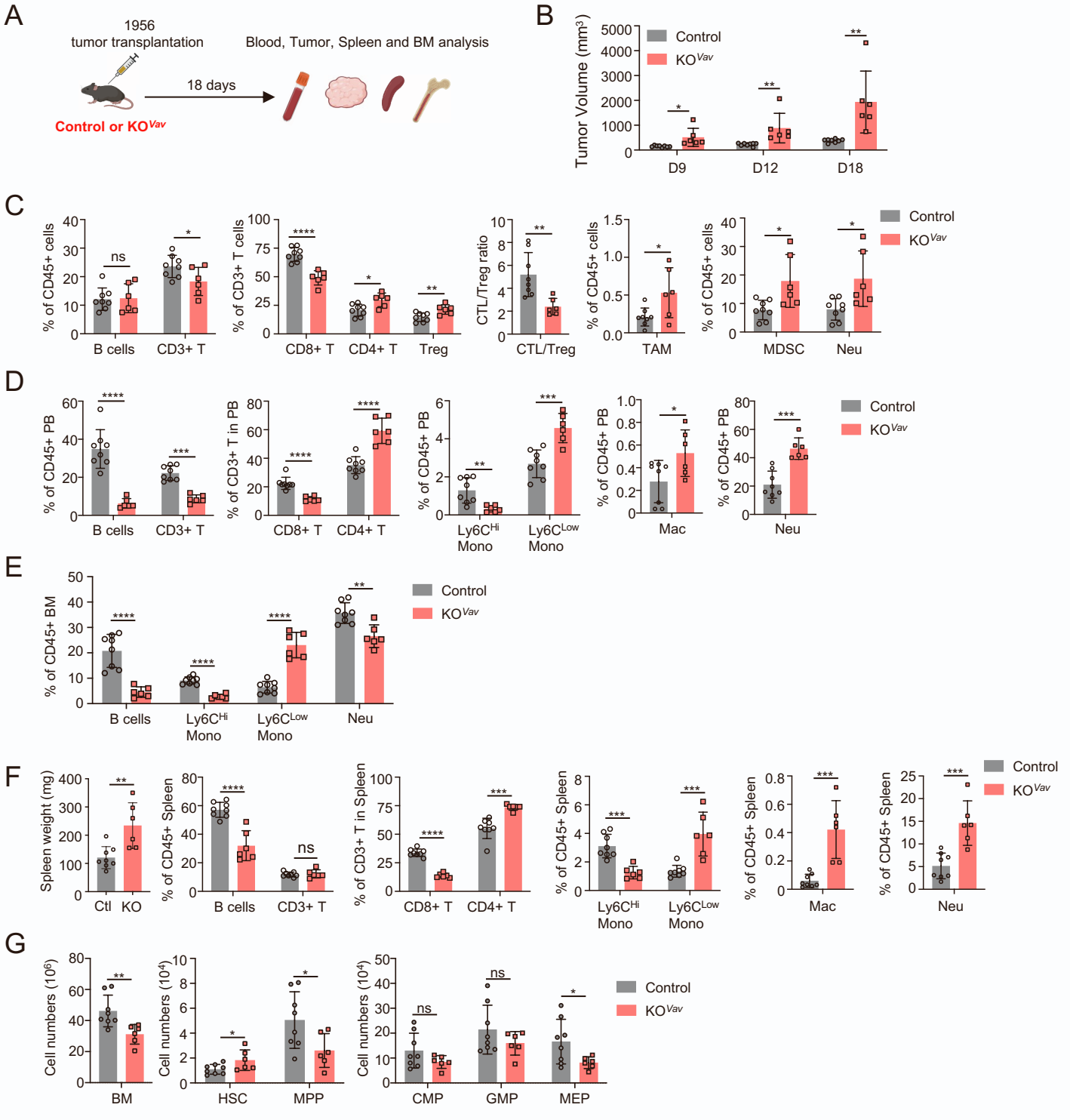

Figure S5. Hematopoietic *Baf155*-deficient mice show more robust tumor progression, related to Figure 5.

(A) Schematic of workflow for the 1956 tumor transplantation.

(B) 1956 tumor growth in control (n=8) and *Baf155 KO^{Vav}* (n=6) mice.

(C) Different immune cell compartments in the tumor of control and *Baf155 KO^{Vav}* mice were analyzed by flow cytometry at endpoints described in (B). Control (n=8) and *Baf155 KO^{Vav}* (n=6).

(D, E and F) Different lineage compartments in the PB **(D),** BM **(E)**, and spleen **(F)** of 1956 tumor-bearing control (n=8) and *Baf155 KO^{Vav}* (n=6) mice were analyzed by flow cytometry at D18.

(G) Cell numbers of different hematopoietic progenitors in the BM of 1956 tumor-bearing control (n=8) and *Baf155 KO^{Vav}* (n=6) mice at D18.

In all relevant panels, each symbol represents an individual mouse. For all graphs, data are presented as mean±SD, the p values were determined by unpaired two-tailed Student's t test. n.s. not significant, *$p<0.05$, **$p<0.005$, ***$p<0.001$, ****$p<0.0001$

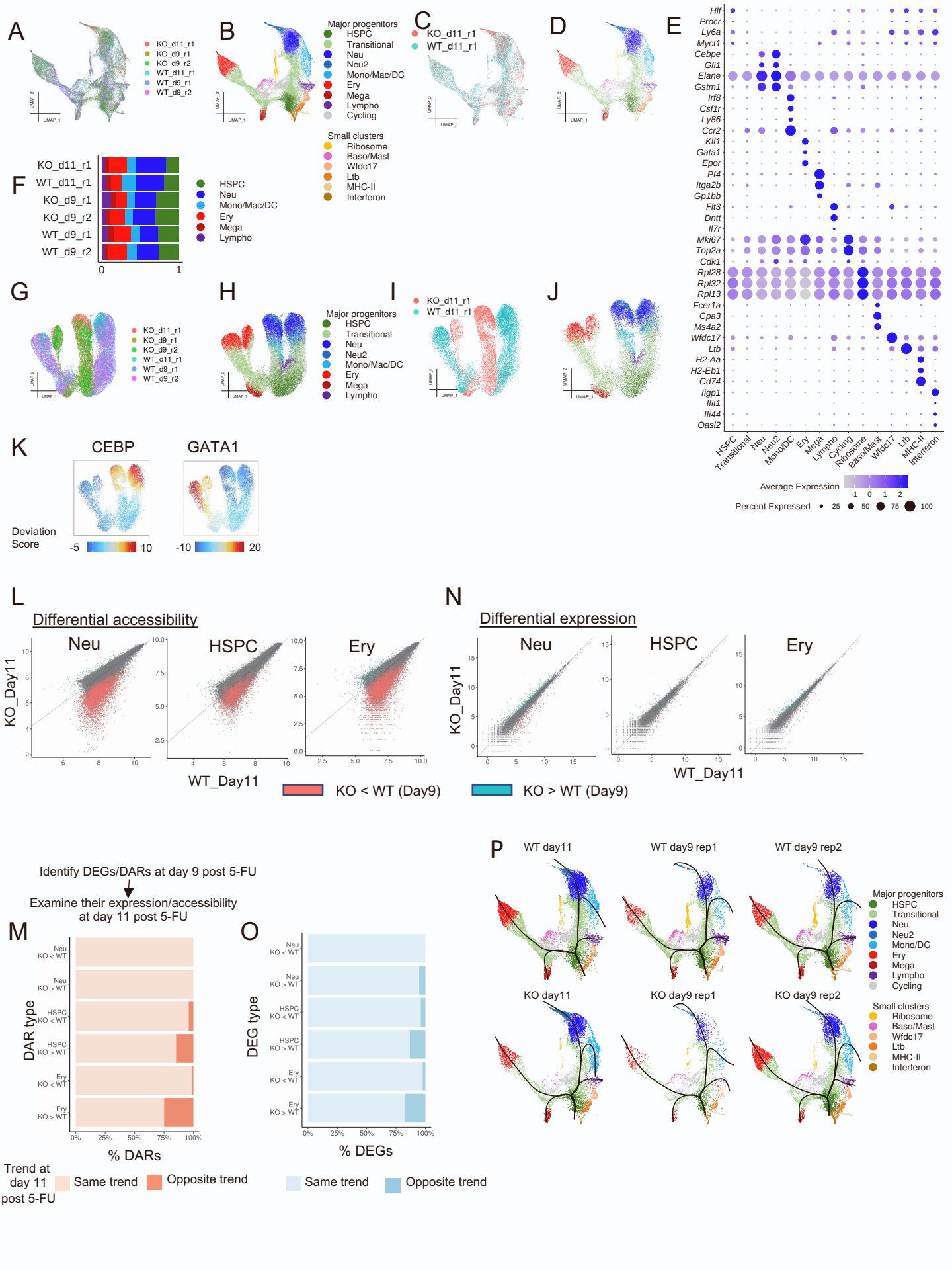
A
KO_d11_r1
KO_d9_r1
KO_d9_r2
WT_d11_r1
WT_d9_r1
WT_d9_r2
B
Major progenitors
HSPC
Transitional
Neu
Neu2
Mono/Mac/DC
Ery
Mega
Lympho
Cycling
Small clusters
Ribosome
Baso/Mast
Wfdc17
Ltb
MHC-II
Interferon
C
KO_d11_r1
WT_d11_r1
D
E
Hlf
Procr
Ly6a
Myct1
Cebpe
Gfi1
Elane
Gstm1
Irf8
Csf1r
Ly86
Ccr2
Klf1
Gata1
Epor
Pf4
Itga2b
Gp1bb
Flt3
Dntt
Il7r
Mki67
Top2a
Cdk1
Rpl28
Rpl32
Rpl13
Fcer1a
Cpa3
Ms4a2
Wfdc17
Ltb
H2-Aa
H2-Eb1
Cd74
Iigp1
Ifit1
Ifi44
Oasl2
HSPC
Transitional
Neu
Neu2
Mono/DC
Ery
Mega
Lympho
Cycling
Ribosome
Baso/Mast
Wfdc17
Ltb
MHC-II
Interferon
Average Expression
-1 0 1 2
Percent Expressed
25 50 75 100
F
KO_d11_r1
WT_d11_r1
KO_d9_r1
KO_d9_r2
WT_d9_r1
WT_d9_r2
0
1
HSPC
Neu
Mono/Mac/DC
Ery
Mega
Lympho
G
KO_d11_r1
KO_d9_r1
KO_d9_r2
WT_d11_r1
WT_d9_r1
WT_d9_r2
H
Major progenitors
HSPC
Transitional
Neu
Neu2
Mono/Mac/DC
Ery
Mega
Lympho
I
KO_d11_r1
WT_d11_r1
J
K
CEBP
GATA1
Deviation Score
-5
10
-10
20
L
Differential accessibility
Neu
HSPC
Ery
KO_Day11
WT_Day11
KO < WT (Day9)
KO > WT (Day9)
N
Differential expression
Neu
HSPC
Ery
KO_Day11
WT_Day11
KO < WT (Day9)
KO > WT (Day9)
Identify DEGs/DARs at day 9 post 5-FU
Examine their expression/accessibility at day 11 post 5-FU
M
DAR type
Neu KO < WT
Neu KO > WT
HSPC KO < WT
HSPC KO > WT
Ery KO < WT
Ery KO > WT
0%
25%
50%
75%
100%
% DARs
O
DEG type
Neu KO < WT
Neu KO > WT
HSPC KO < WT
HSPC KO > WT
Ery KO < WT
Ery KO > WT
0%
25%
50%
75%
100%
% DEGs
Trend at day 11 post 5-FU
Same trend
Opposite trend
Same trend
Opposite trend
P
WT day11
WT day9 rep1
WT day9 rep2
KO day11
KO day9 rep1
KO day9 rep2
Major progenitors
HSPC
Transitional
Neu
Neu2
Mono/DC
Ery
Mega
Lympho
Cycling
Small clusters
Ribosome
Baso/Mast
Wfdc17
Ltb
MHC-II
Interferon

Figure S6. Transcriptomic and chromatin accessibility landscapes of WT and *Baf155 KO* HSPCs at day 9 and 11 post 5-FU treatment, related to Figure 6.

(A) UMAP based on the RNA fraction of multiomic data from all cells (day 9 and 11), colored by sample.

(B) UMAP based on the RNA fraction of the multiomic data from all cells (day 9 and 11), colored by cell type.

(C-D) Same as **A-B**, but with day 11 cells only.

(E) Dot plot of the marker genes used to identify hematopoietic clusters. Color: expression level, scaled across each row. Dot sizes: percentage of cells expressing the gene for each cluster.

(F) Relative sizes of major clusters in each sample. The number and fraction of cells in each population for each sample are in **Table S1**.

(G) UMAP based on the ATAC fraction of the multiomic data (day 9 and 11), colored by samples.

(H) UMAP based on the ATAC fraction of the multiomic data (day 9 and 11), colored by cell types defined in **B**. Clusters with small number of cells were removed.

(I-J) same as **G-H**, but with day 11 cells only.

(K) Smoothed chromVAR (Methods) results depicting the enrichment (high deviation score) or depletion (low deviation score) of chromatin accessibility in peaks containing CEBP or GATA1 motif on a single cell basis. Only day 11 cells are shown.

(**L**) Scatter plot of chromatin accessibility at each peak (KO day 11 against WT day 11). Each dot represents a peak in the cluster-specific peak x sample pseudobulk matrix. The same set of peaks were used for day 9 (**Figure 7A**) and day 11 samples. DARs from the day 9 comparison were colored (i.e., colored dots represent the same peaks as **Figure 7A**).

(**M**) For up-DARs (KO > WT) defined at day 9 post 5-FU (**Figure 7A**), “same trend” indicates those that also showed higher accessibility in KO at day 11, whereas “opposite trend” indicates those that showed lower accessibility in KO at day11. Down-DARs were analyzed similarly.

(**N-O**) same as **L-M** but showing DEGs instead.

(**P**) Hematopoietic trajectories constructed using Slingshot (**Methods**). The PCA space (PC1-30, based on RNA data) was used.

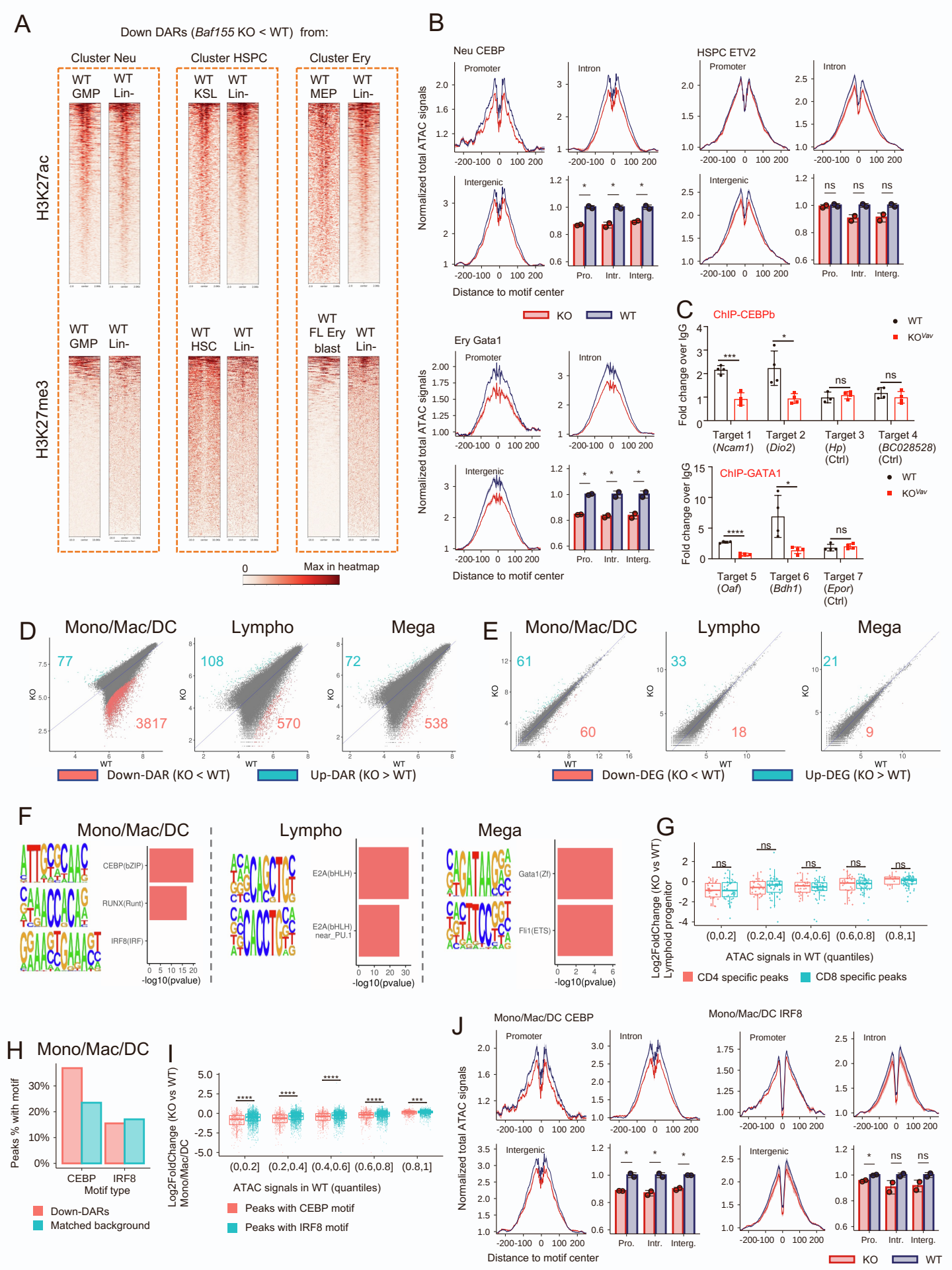
A
Down DARs (Baf155 KO < WT) from:
Cluster Neu
Cluster HSPC
Cluster Ery
WT GMP
WT Lin-
WT KSL
WT MEP
H3K27ac
H3K27me3
WT HSC
WT FL Ery blast
0
Max in heatmap
B
Neu CEBP
HSPC ETV2
Promoter
Intron
Intergenic
Normalized total ATAC signals
Distance to motif center
Pro.
Intr.
Interg.
KO
WT
Ery Gata1
C
ChIP-CEBPb
ChIP-GATA1
Fold change over IgG
KOVav
Target 1 (Ncam1)
Target 2 (Dio2)
Target 3 (Hp) (Ctrl)
Target 4 (BC028528) (Ctrl)
Target 5 (Oaf)
Target 6 (Bdh1)
Target 7 (Epor) (Ctrl)
D
Mono/Mac/DC
Lympho
Mega
77
3817
108
570
72
538
Down-DAR (KO < WT)
Up-DAR (KO > WT)
E
61
60
33
18
21
9
Down-DEG (KO < WT)
Up-DEG (KO > WT)
F
CEBP(bZIP)
RUNX(Runt)
IRF8(IRF)
E2A(bHLH)
E2A(bHLH) near_PU.1
Gata1(Zf)
Fli1(ETS)
-log10(pvalue)
G
Log2FoldChange (KO vs WT) Lymphoid progenitor
ATAC signals in WT (quantiles)
CD4 specific peaks
CD8 specific peaks
H
Mono/Mac/DC
Peaks % with motif
CEBP
IRF8
Motif type
Down-DARs
Matched background
I
Log2FoldChange (KO vs WT) Mono/Mac/DC
ATAC signals in WT (quantiles)
Peaks with CEBP motif
Peaks with IRF8 motif
J
Mono/Mac/DC CEBP
Mono/Mac/DC IRF8

Figure S7. *Baf155* regulates chromatin accessibility at hematopoietic lineage transcription factor binding loci, related to Figure 7.

(A) Pile-up heatmaps of H3K27ac and H3K27me3 profiles. For each cell type, 500 randomly sampled down-DARs not overlapping repetitive elements were used. 2kb and 10kb flanking regions up and downstream of peak centers were plotted for H3K27ac and H3K27me3, respectively. Original bigWig tracks uploaded by authors of the following works were used:

For H3K27ac: Lin- cells, Yun et al., 2021 [S1] ; GMPs, Poplineau et al., 2019 [S2]; KSL, Antoszewski et al., 2022 [S3]; MEP, Hu et al., 2019 [S4].

For H3K27me3: Lin- cells, Man et al., 2021 [S5]; GMP, Poplineau et al., 2019 [S2]; HSC, Celik et al., 2018 [S6]; FL erythroblast, Ling et al., 2019 [S7].

(B) ATAC signal pile-up signatures at the motif instances of selected transcription factors. Solid lines represent the mean of 2 replicates for each genotype. Shaded regions represent standard deviation. ATAC pile-up signatures were partitioned into “Promoter”, “Intronic”, or “Intergenic” categories (**Methods**). n = 2 biological replicates (separate pools of mice) for each genotype. The ATAC signature was quantified as the mean pile-up value within the motif center ± 25 bp region and presented in bar plots. Values are normalized so that the mean value for WT samples is 1. Means (bars) and individual values (points) are shown. Error bars: mean ± s.d. Two-tailed unpaired Student’s *t*-test. P values were corrected within each bar plot. ns: FDR >= 0.05; *FDR < 0.05.

(C) ChIP-qPCR data measuring the differential binding of CEBPb or GATA1 in down-DARs of Ery or Neu clusters, respectively, together with non-DAR controls. The locations of targets and the sequences of primers are in **Table S6**. The gene names indicate the closest gene of each DAR. Control (n=4) and *Baf155 KO^{Vav}* (n=4) mice. For all graphs, data are presented as mean±SD, the p values were determined by unpaired two-tailed Student’s t test. n.s. not significant, **p<0.05, ***p<0.001, ****p<0.0001.*

(D) DAR analysis, same as **Figure 7A**, but for Mono/Mac/DC, lymphoid, and megakaryocytic progenitors.

(E) DEG analysis, same as **Figure 7E**, but for Mono/Mac/DC, lymphoid, and megakaryocytic progenitors.

(F) TF motif enrichment in down-DARs (calculated by HOMER), same as **Figure 7B**, but for Mono/Mac/DC, lymphoid, and megakaryocytic progenitors.

(G) The log2 fold changes of CD4 or CD8-specific peaks in KO vs WT lymphoid progenitors. See “**Bulk ATAC-seq library generation and data analyses**” for details. Two-tailed unpaired Student’s *t*-test. ns: FDR >= 0.05. Error bars: mean ± s.d. For CD4 specific peaks, n = 35, 27, 28, 28, and 10 peaks for each quantile, respectively. For CD8 specific peaks, n = 43, 50, 49, 49, and 68 peaks for each quantile, respectively.

(H) The percentage of down-DARs in KO Mono/Mac/DC progenitors with the CEBP or IRF8 motif, compared to non-DARs with similar accessibility levels in WT cells (matched background). This is the source data of the p values shown in **(F)**, and parsed from HOMER outputs.

(I) The log2 fold changes of Mono/Mac/DC peaks with CEBP or IRF8 motifs (KO vs WT). Motif occurrences were determined by ArchR (ArchR::addMotifAnnotations). Log2 fold changes were calculated by DESeq2 as a part of the pseudobulk-based ATAC analyses. Two-tailed unpaired Student’s *t*-test. ***FDR < 0.001; ****FDR < 0.0001. Error bars: mean ± s.d. For peaks with the CEBP motif, n = 463, 459, 470, 524, and 448 peaks for each quantile, respectively. For peaks with the IRF8 motif, n = 1834, 1744, 1770, 1717, and 1793 peaks for each quantile, respectively.

(J) ATAC signal pile-up, same as **Figure S7B**, but for Mono/Mac/DC progenitors.

References

1. Yun, H., Narayan, N., Vohra, S., Giotopoulos, G., Mupo, A., Madrigal, P., Sasca, D., Lara-Astiaso, D., Horton, S.J., Agrawal-Singh, S., et al. (2021). Mutational synergy during leukemia induction remodels chromatin accessibility, histone modifications and three-dimensional DNA topology to alter gene expression. Nat Genet *53*, 1443-1455. 10.1038/s41588-021-00925-9.
2. Poplineau, M., Vernerey, J., Platet, N., N'Guyen, L., Herault, L., Esposito, M., Saurin, A.J., Guilouf, C., Iwama, A., and Duprez, E. (2019). PLZF limits enhancer activity during hematopoietic progenitor aging. Nucleic Acids Res *47*, 4509-4520. 10.1093/nar/gkz174.
3. Antoszewski, M., Fournier, N., Ruiz Buendia, G.A., Lourenco, J., Liu, Y., Sugrue, T., Dubey, C., Nkosi, M., Pritchard, C.E.J., Huijbers, I.J., et al. (2022). Tcf1 is essential for initiation of oncogenic Notch1-driven chromatin topology in T-ALL. Blood *139*, 2483-2498. 10.1182/blood.2021012077.
4. Hu, T., Morita, K., Hill, M.C., Jiang, Y., Kitano, A., Saito, Y., Wang, F., Mao, X., Hoegenauer, K.A., Morishita, K., et al. (2019). PRDM16s transforms megakaryocyte-erythroid progenitors into myeloid leukemia-initiating cells. Blood *134*, 614-625. 10.1182/blood.2018888255.
5. Man, N., Mas, G., Karl, D.L., Sun, J., Liu, F., Yang, Q., Torres-Martin, M., Itonaga, H., Martinez, C., Chen, S., et al. (2021). p300 suppresses the transition of myelodysplastic syndromes to acute myeloid leukemia. JCI Insight *6*. 10.1172/jci.insight.138478.
6. Celik, H., Koh, W.K., Kramer, A.C., Ostrander, E.L., Mallaney, C., Fisher, D.A.C., Xiang, J., Wilson, W.C., Martens, A., Kothari, A., et al. (2018). JARID2 Functions as a Tumor Suppressor in Myeloid Neoplasms by Repressing Self-Renewal in Hematopoietic Progenitor Cells. Cancer cell *34*, 741-756 e748. 10.1016/j.ccell.2018.10.008.
7. Ling, T., Birger, Y., Stankiewicz, M.J., Ben-Haim, N., Kalisky, T., Rein, A., Kugler, E., Chen, W., Fu, C., Zhang, K., et al. (2019). Chromatin occupancy and epigenetic analysis reveal new insights into the function of the GATA1 N terminus in erythropoiesis. Blood *134*, 1619-1631. 10.1182/blood.2019001234.